Observations and modeling of heat fluxes on tidal flats

J. P. Rinehimer,[1,2], and Jim T. Thomson[1,2]

Corresponding author: J. P. Rinehimer, Applied Physics Laboratory, University of Washington, 1013 NE 40th St, Seattle, WA 98105, USA. (jprine@apl.washington.edu)

[1]Applied Phyiscs Laboratory, University of Washington, Seattle, Washington, USA.

[2]Department of Civil and Environmental Engineering, University of Washington, Seattle, Washington, USA.

Abstract. A cross-shore model of tidal flat heat and mass fluxes is developed to understand the heat exchange between the sediment bed and the water column. A convective heat-transfer coefficient is used to model sediment-water heat fluxes which are as great as 20% of the incoming solar shortwave radiation. The model results match well with observations and are used to assess processes accross tidal to seasonal timescales. During the summer, tidal flat sediments store incoming shortwave radiation during exposure and act effectively as a net source of heat to the water column. This pattern changes in the winter, when the flats cool during exposure and act effectively as a net sink of heat. Additionally, during the summer water temperatures at the edge of the flooding front are elevated 5 °C above the surface sediment temperatures. Model results replicate this process only when water column light extinction coefficients are high, consistent with visual observations of high turbidity (and thus high light absorption) at the leading edge of the flooding front.

1. Introduction

Tidal flats occur in regions of significant sediment supply and are a common feature of estuaries and coastlines worldwide. Characterized by large intertidal areas with strong tidal forcing relative to wave forcing, these regions contain high levels of benthic microalgal biomass and production, which supply the base of coastal food webs [*Colijn and de Jonge*, 1984]. Tidal flats are important habitats for migratory birds, commercially valuable young fishes such as salmon, and highly productive bivalve fisheries. Tidal flats also present significant navigational hazards for ships entering coastal ports and provide much of the area for land reclamation projects.

While much research has been focused on tidal flat hydrodynamics, sediment transport, and morphodynamics [See *Amos*, 1995; *Friedrichs*, 2012, for reviews.], thermodynamics in these systems is not as well understand. Water temperatures often control rates of biogeochemical processes like nutrient cycling and primary productivity [*Guarini et al.*, 1997]. Alternating inundation and exposure of large regions of tidal flats suggest that differences between the thermodynamic properties of water and sediments may also play an important role in local climate and weather [*Cho et al.*, 2000]. An understanding of the local heat budgets of these systems is also important when determining the impacts of significant sources of thermal pollution such as nuclear power facilities. [*Yanagi et al.*, 2005].

Solar radiation represents the most important external forcing of tidal flat temperatures. *Losordo and Piedrahita* [1991] developed a numerical model to study the thermal structure of aquaculture ponds. During the spring, incident solar radiation heated the lake surface resulting in thermal stratification. There was sufficient mixing within the lake, however, such that heat exchange between the sediment and water column was important in determining the thermal budget. Warm water was mixed from above and the sediment bed acted as a net sink of heat. This was reversed during the fall when diminished solar radiation and lower air temperatures resulted in the mixing of cold water to depth and the loss of heat from the sediment bed to the water column.

Similar seasonal cycles are apparent on tidal flats as well as in aquaculture ponds. *Kim et al.* [2010] found that during spring local solar heating of exposed tidal flats in Baeksu, Korea caused temperature differences of 2 °C – 4 °C between the sediment surface and water column temperatures. Inversely, during the winter and limited incident solar radiation, exposed sediment temperatures were lower than water column temperatures with the coldest seawater temperatures occurring in the shallow regions of the embayment. These differences between sediment and water column temperatures create thermal gradients that drive heat exchange between the seabed and water column. Net heat transfer between the water and the sediment is thus determined by the phasing of solar shortwave radiation and periods of exposure of the tidal flats.

The study of *Kim et al.* [2010] used a similar method to that of *Losordo and Piedrahita* [1991] to calculate the net heat flux between the sediment bed and the water column. They assume an effective sediment thickness (H_{sed}) over which heat exchange occurs to calculate the net sediment-water heat flux, following

$$Q_{sw} = C_s \frac{2\kappa}{H_{sed}} (T_w - T_s) \quad (1)$$

where Q_{sw} is the sediment-water heat exchange, T_w is the water temperature, T_s is the sediment surface temperature, H_{sed} is the 'effective' sediment thickness, and κ and C_s

are the thermal diffusivity and volumetric specific heat capacity of the seabed. Values for H_{sed} are usually not given, however, nor are empirical methods of their determination presented. While the effective thickness seems to be reasonable for sediments that are always inundated, it may be inappropriate for the dynamic depth changes occurring on tidal flats. These prior studies also required the specification of sediment temperatures at depth in order to accurately replicate their observations. Given that the major forcing for tidal flat areas is from surface heating and offshore advection, accurate predication of tidal flat temperatures should be possible without knowledge of the absolute temperatures at depth.

This study adapts the previous work and aims to improve thermodynamic process modeling for tidal flats. The results of in-situ measurements and modeling studies are described at two locations: Skagit Bay and Williapa Bay, Washington, USA during summer and winter 2009. The field data is used to calibrate and force a one-dimensional, cross-flat model of tidal flat mass and heat fluxes including heat exchange between the tidal flat sediment and water column. Times scales of seasonal, fortnightly, and tidal variations are addressed. Estimates of net sediment-water heat fluxes for each season are determined and the sensitivity of the fluxes to sediment and water parameters is evaluated. Small-scale heating processes at the flooding front are then examined to determine local heating during the summer months.

2. Methods

2.1. Study Sites and Field Observations

Field observations and model calculations were performed for two tidal flats in Washington State, USA: Skagit Bay and Willapa Bay (Figure 1). Willapa bay is a bar-built embayment on the Pacific Coast with a tidal range varying from 1.8 m to 3.7 m between neap and spring tides. Nearly half of the bay's surface area is intertidal [*Andrews*, 1965]. The study sites are located in the southern portion of Willapa Bay in sediments consisting of primarily silt and clay. [*Boldt et al.*, 2013].

Skagit Bay, located 230 km to the northeast of Willapa Bay, is a sub-embayment of Puget Sound and the receiving basin for the Skagit River. Sediment deposits at the mouth of the Skagit River form a large intertidal delta with sand occurring nearshore and grain size fining southwestward, away from the mouth. Fine grained sediments are also located in sheltered areas north of the Swinomish Channel [*McBride et al.*, 2006].

Sediment and water temperature observations were collected at both bays spanning a (non-continuos) period of two years (2009-2010). Hobo TempPro v2 temperature loggers affixed to a metal sand anchor recorded temperatures in the sediment bed, spaced at 10 cm intervals spanning 10 - 50 cm depths in the sediment. At the sediment surface, a Hobo U20 water level logger measured water depth and surface temperatures. An additional TempPro logger attached to a length of nylon rope measured near-bed water temperatures during inundation at 10 cm above the sediment surface. The temperature loggers recorded at 5 min intervals, over twice the response time of the loggers, and have an accuracy of ± 0.2 °C with a resolution of 0.02 °C. Prior studies by *Thomson* [2010] have shown minimal effects due to heat conduction down the sand anchor and disturbance of the sediment bed during deployment with a RMS deviation of <0.15 °C between plastic and metal sand anchors. This variance is small compared to the ±10 °C variations seen in the daily temperatures.

A HOBO U30 meteorological station located near the study sites collected 5 minute observations of air temperature, wind speed and direction, solar shortwave radiation, and relative humidity. The meteorological station was attached to a 1.5 m tripod and located on the nearby Craft Island at 28 m elevation while at Willapa Bay it was affixed to a piling near Round Island at 7 m elevation. Nearby Washington State University AgWeatherNet stations at Long Beach (Willapa Bay) and Fir Island (Skagit Bay) were used to provide meteorological data during brief data gaps. Hourly METAR reports from nearby airports in Astoria OR (KAST) and Burlington, WA (KBVS) provided observations of cloud cover. As METAR observations report cloud cover values in oktas at various elevations, the maximum okta value over all reported elevations for each hourly report was used to determine the percent cloud cover.

2.2. Numerical model

A 1-dimensional (cross-flat) numerical model, following *Kim et al.* [2010], was developed to simulate the tidal wetting and drying of the flats and the heat fluxes to the water and sediment. The model considers horizontal, cross-flat advection of mass and heat as well as the vertical diffusion of heat in the sediment bed. The cross-flat resolution is 50 m and the water column is represented by a single, vertically homogenous cell at each cross-flat location. *Pavel et al.* [2012] indicate that some stratification occurs on the flats, however, it is generally intermittent, occurring when the leading edge of the flood or ebb tidal front pass over the site. Mass and heat fluxes are assumed to be dominated by advective processes and cross-flat diffusion is not modeled. Along flat processes are also ignored. Model bathymetry H^i is assigned according to the average slope of the flats, about 0.79

m/km at Skagit Bay and 0.76 m/km at Willapa Bay. The offshore boundary depth was -5 m (MLLW) for each site.

2.2.1. Water column model

The model is forced at the open boundary by a tidally varying sea surface elevation η_t. Assuming a constant water elevation over the modeled domain allows calculation of the mass flux and velocity using only the continuity equation:

$$F_t^i = \sum_{k=i}^{M} \left(\frac{\eta_t - \eta_{t-\Delta t}}{\Delta t} \right) dx \tag{2}$$

where F_t^i is the volume flux between cells $i-1$ and i at time t, Δt is the time-step size, dx is horizontal cell size, and M is the total number of cross-channel cells in the domain. No fluxes are permitted through the onshore boundary. Subscripts indicate time indices while superscripts indicate spatial indices.

The water temperature $T_{w,t}^i$ at location i and time t is calculated by:

$$T_{w,t}^i = \Delta T_{local} + \Delta T_{adv} + \Delta T_{ext} \tag{3}$$

where ΔT_{local} is the local change in temperature due to the changing cell size (i.e. water elevation), ΔT_{adv} is due to the advective heat flux, and ΔT_{ext} is due to the external heat fluxes through the water surface or sediment-water interface. The local and external terms are calculated through first order, backward differences (in time) as

$$\Delta T_{local} = T_{w,t-\Delta t}^i \frac{H^i + \eta_{t-\Delta t}}{H^i + \eta_t} \tag{4}$$

$$\Delta T_{ext} = \frac{Q_{w,t}^i \Delta t}{C_w \left(H^i + \eta_t \right)} \tag{5}$$

where C_w is the volumetric heat capacity of water and $Q_{w,t}^i$ is the net heat flux into the water column (see below).

The advective term depends on the flow direction and is determined by

$$\Delta T_{adv} = \begin{cases} \left(T^{i-1}_{w,t-\Delta t} F^{i}_{t} - T^{i}_{w,t-\Delta t} F^{i+1}_{t}\right) \frac{\Delta t}{dx(H^i+\eta_t)} & \text{during flood} \\ \left(T^{i}_{w,t-\Delta t} F^{i}_{t} - T^{i+1}_{w,t-\Delta t} F^{i+1}_{t}\right) \frac{\Delta t}{dx(H^i+\eta_t)} & \text{during ebb} \end{cases} \quad (6)$$

At the open boundary, an offshore water temperature T_{sea} is specified while no fluxes occur through the landward boundary.

2.2.2. Sediment model

Vertical transport of heat within the sediment bed is modeled at each x-location according to the diffusion equation

$$\frac{dT}{dt} = \kappa \frac{dT_s^2}{d^2 z} \quad (7)$$

where κ is the thermal diffusivity of the sediment and T_s is the sediment temperature, which varies with depth. The diffusion equation is solved at each modeled cross-flat location and no horizontal mixing is allowed between locations. Eq. 7 is modeled using a 2$^{\text{nd}}$-order Rung-Kutta method. The lower boundary condition assumes that dT/dz is constant with the layer above, while the boundary at the surface interface is given by

$$Q_s = \lambda_s \frac{dT}{dz}\bigg|_{z=0} \quad (8)$$

where Q_s is the heat flux through the surface and λ_s is the thermal conductivity of the sediment. The bed is modeled from the surface down to 2 m depth with 10 cm vertical resolution.

Thermal diffusivity κ and conductivity λ_s depend on the the sediment type, porosity, and water content [*Thomson*, 2010]. *Kim et al.* [2007] summarize prior studies with values of κ between 0.4-1.1 $\times 10^{-6}$ m^2 s^{-1} and λ between 0.8-3.1 W m^{-1} K^{-1}. For this study, $\kappa = 1.0 \times 10^{-6}$ m^2 s^{-1} was chosen for the Skagit Bay site and $\kappa = 0.5 \times 10^{-6}$ m^2 s^{-1} was chosen for Willapa Bay based on *Thomson* [2010] which found values of κ between 0.6-1.4

$\times 10^{-6}$ m^2 s^{-1} for Skagit Bay sand and 0.4-0.6 $\times 10^{-6}$ m^2 s^{-1} for Willapa Bay mud. A range of conductivities between $\lambda = 1 - 10$ W m^{-1} K^{-1} [*Thomson*, 2010] were used to tune the model and test sensitivity.

2.2.3. Heat fluxes

The net heat flux into the water column (Q_w) or the sediment (Q_s) is determined by

$$Q_w = Q_{ws} + Q_{wl} + Q_{wh} + Q_{we} + Q_{sw} \tag{9}$$

$$Q_s = Q_{ss} + Q_{sl} + Q_{sh} + Q_{se} - Q_{sw} \tag{10}$$

where Q_{xs} is the net shortwave radiation, Q_{xl} is the net long wave radiation, Q_{xh} is the sensible heat flux, Q_{xe} is the latent heat flux, and the first subscript x indicates whether the flux is to the sediment (s) or the water column (w). Solar shortwave radiation is calculated according to

$$Q_{sn} = (1 - \alpha_x) Q_{s0} \tag{11}$$

where Q_{s0} is the incoming shortwave radiation, Q_{sn} is the net shortwave radiation, and α_x is the albedo of the appropriate substance. Despite seasonal variations in albedo due to changing solar angle [*Kim et al.*, 2007], constant mean values of $\alpha_s = 0.20$ and $\alpha_w = 0.05$ were used for the model [*Thomson*, 2010].

During exposure of the flats, all net shortwave radiation is absorbed by the sediment bed such that $Q_{ss} = Q_{sn}$. During inundation, however, not all of the net radiation is absorbed by the water, and some of the incident solar shortwave radiation may reach the seabed. The fraction of radiation that reaches the bed can be computed by the Beer-Lambert law:

$$T = e^{-K_d d} \tag{12}$$

where d is the depth, T is the transmissivity, and K_d is the extinction coefficient. The amount of shortwave radiation that is absorbed by the water column is $Q_{ws} = (1-T)Q_{sn}$ and the seabed $Q_{ss} = TQ_{sn}$. The extinction coefficient varies as a function of wavelength, with longer wavelength radiation generally having higher extinction coefficients [*Jerlov*, 1976]. Extinction coefficients of 1-25 m^{-1} are common for moderate turbidities from 10-100 mgL^{-1} within the 400 μm-700 μm photosynthetically active radiation (PAR) range [*Stefan et al.*, 1983]. Nearly half of the solar shortwave radiation is outside this range, however, and within the more quickly attenuating IR range. Studies of the Hudson River plume indicate values of K_d >100 m^{-1} within the plume [*Cahill et al.*, 2008]. For this study, a bulk value for all wavelengths will be used to estimate the qualitative impacts of absorption coefficient.

The long-wave heat flux, Q_{xl} is calculated following *May* [1986]

$$Q_{xl} = \left[\epsilon\sigma T_a^4\left(0.4 - 0.05e_a^{1/2}\right) + 4\epsilon\sigma T_a^3\left(T_x - T_a\right)\right]\cdot\left(1 - 0.75C^3.4\right) \tag{13}$$

where ϵ is the emisivity, σ is the Stefan-Boltzmann constant ($5.6705\times10^{-8}\mathrm{Wm}^{-2}\mathrm{K}^{-4}$), T_a is the air temperature, C is the fractional cloud cover from 0-1, and T_x is the water temperature T_w or the sediment surface temperature T_s.

Calculation of sensible heat transfer, Q_{xh} is given by *Guarini et al.* [1997]:

$$Q_{xh} = \rho_a C_{Pa} C_h \left(1 + U\right)\left(T_x - T_a\right) \tag{14}$$

where ρ_a is the density of air, C_{Pa} is the specific heat of air at standard pressure, C_h is the bulk transfer coefficient for conduction, and U is the wind speed in m/s.

Latent heat transfer, Q_{xe} is given following *Guarini et al.* [1997]:

$$Q_{se} = \xi V_s \tag{15}$$

$$Q_{we} = V_w \tag{16}$$

where ξ is the water content of the flat surface with V_s and V_w defined as:

$$\begin{aligned} V_x &= \rho_a L_V C_v \left(1 + U\right)\left(q_x - q_a\right) && (17)\\ L_V &= \left[2500.84 - 2.35\left(T_x - 273.15\right)\right] \times 10^3 && (18)\\ q_s &= \frac{\lambda p^V_{sat}}{p_{atm} - (1-\lambda)p^V_{sat}} && (19)\\ p^V_{sat} &= \exp\left\{2.3\left[\frac{7.5\left(T_x - 273.15\right)}{237.3 + \left(T_x - 273.15\right)} + 0.76\right]\right\} && (20) \end{aligned}$$

where ρ_a is the density of air (1.29 kg m^{-3}), C_v is the bulk transfer coefficient for conduction (0.0014), U is the wind speed (m s^{-1}) at 10 m, L_v is the latent heat of evaporation, q_s is the specific humidity of saturated air at the (pore) water temperature, q_a is the absolute air humidity, p_{atm} is the atmospheric pressure and p^V_{sat} is the saturation vapor pressure

The heat flux through the sediment-water interface is denoted by $Q_{sw}$where positive values indicate heat flux to the water column and negative values indicate heat flux to the sediment. The sediment-water heat flux is estimated using a convective heat-transfer coefficient h_{sw} [*Incropera and DeWitt*, 2002]

$$Q_{sw} = h_{sw}\left(T_s - T_w\right) \tag{21}$$

Previous studies [*Kim et al.*, 2010; *Losordo and Piedrahita*, 1991] have used a formulation of Q_{sw} which requires the determination of an effective sediment thickness, however, no guidance for the determination this parameter is presented. The use of a heat-transfer coefficient is common in convective transfer between a fluid and a solid [*Incropera and DeWitt*, 2002] and is straightforward to estimate empirically.

Estimations of h_{sw} were obtained by the "heat storage" method [*Harrison*, 1985]. To determine the change in heat content of the sediment bed, observations of sediment temperature with depth were integrated vertically according to:

$$Q_{sw} = \frac{\partial}{\partial t} \int_{z_0}^{0} C_v T(z) dz + \lambda_s \frac{\partial T}{\partial z}\bigg|_{z_0} \tag{22}$$

where C_v is the volumetric heat capacity of the sediment bed, λ_s is the thermal conductivity of the sediment, and z_0 is the depth of integration into the bed. The first term of the right hand side of Eq. 22 represents the change in storage of heat in the upper portion of the sediment bed while the second term represents the flux of heat into the lower layers. $z_0 = 0.5$ m was taken as the lowest elevation of the sediment temperature measurements. Eq. 22 was discritized by a forward difference in time and a backward difference at $z = z_0$ to estimate heat transfer below z_0. h_{sw} was then estimated by fitting:

$$Q_{sw} = \frac{\Delta H_{sed}}{\Delta T} = h_{sw} \left(T_{sed} - T_w\right) \tag{23}$$

where H_{sed} was calculated using Eq. 22. Regressions were performed at each field location using the full time series of observations (Nov. 2008 – Sept. 2009) and by binning the data into 0.1 °C ΔT bins. Conditions were limited to periods of inundation were the depth was greater than 1 m in order to eliminate the potential interference of solar radiation reaching the bottom of the water column and providing an extra heat source to the sediment bed.

Examples of these regressions are shown in Figure 2 for characteristic sites at both Skagit Bay (Figure 2a) and Willapa Bay (Figure 2b). Values of h_{sw} for both Skagit and Willapa Bays range from 2.0 to 20 W m^{-2} K^{-1}, depending on the composition of a specific location. ΔH_{sed} and ΔT were well correlated at both sites with $r^2 = 0.86$ for Skagit Bay and $r^2 = 0.85$ for Willapa Bay.

3. Results

Each location was modeled for 15-20 days during the winter and summer months in order to observe the spring-neap tidal cycle. Model time periods were based on observational time periods. The summer model time period for Skagit Bay was from 7-27 July 2009 and the winter period was from 9-29 January 2009. For Willapa Bay, the summer modeled time period was from July 2009 and, due to the unavailability of winter data, the "winter" run was during March 2009.

Figure 3 shows the observations and model results of water and sediment temperatures for Skagit Bay during summer 2009 (9-24 July). The strong summer solar shortwave radiation drives the sediment and water column temperatures during this time period. A fortnightly signal is evident, which is specific to the seasonal modulation of tidal phasing in the Pacific Northwest. During the spring tides (9-11 and 21-23 July), exposure of the seabed occurs during the day causing the surface of the flats to absorb the incident solar radiation and heat up. The heat then diffuses vertically down into the sediment. When the site becomes inundated, with cooler water above the surface of the flats, heating stops and the sediment cools as heat is conducted into the water column (i.e. Q_{sw} positive). During the neap tides (13-18 July), daytime exposures are brief and hence the sediments do not warm up. Instead the water column absorbs the solar shortwave radiation and Q_{sw} is then directed into the sediment. These sediment-water heat fluxes are generally 10-20% of the incoming solar-shortwave radiation.

The tidal phasing is reversed in the winter, and cooling results, as shown in Figure 4. In the winter spring tides, tidal flat exposure occurs during the night when no solar shortwave radiation is incident on the flats. This exposure leads to cooling of the sediments and the subsequent inundation of warmer water over cold flats. Sediment-water heat fluxes are then directed towards the sediment bed during this entire time period. These sediment-water heat fluxes are generally of the same order as the solar shortwave fluxes and are important after sunset when shortwave input vanishes.

For both seasons the model accurately represents the sediment temperatures. The root-mean-square errors (RMSE) in sediment temperature are 2.72 °C and 3.98 °C for the summer and winter, respectively. The RMSE in water temperatures is 2.54 °C for the summer; no water temperature data was available for the winter. These errors are small relative to the 20 °C diurnal variations. The model is unable to reproduce some of the higher frequency variability (e.g., during the summer neap tides 13-18 July). This is likely due to circulation and along-flat variations, including changes in offshore temperature and river input.

Similar patterns are apparent at the Willapa Bay site for summer (July 21-28), as shown in Figure 5. Strong solar shortwave radiation heats up the exposed flats during summer low tides. The Willapa site has greater exposure during the smaller semidiurnal tide than the Skagit site due to the larger diurnal inequality in Puget Sound than on the coast. Minimal cooling occurs during these smaller tides, however, and the dominate summer time signal is the heating of the tidal flats. During the late winter (March 2-22), shown in Figure 6, night time cooling dominates the sediment temperatures causing sediment-water fluxes to be directed towards the sediment bed. Model RMSEs are 4.46 °C and 2.9 °C for the summer and winter water temperatures and 3.56 °C and 0.96 °C for the summer and winter sediment temperature, respectively. Despite the similar magnitude of Q_{s0} during July and March, Q_{sw} is directed into the sediment bed (from the water) for most of the winter results, because the exposure of the flats and high daytime shortwave radiation are out of phase.

3.1. Cumulative Heat Fluxes by Season

To determine the long-term influence of sediment-water heat fluxes on the water column, Q_{sw} was integrated over each of the modeled periods for the the summer and winter cases. The cumulative heat fluxes for Skagit Bay are shown in Figure 7. During the summer, the sediment acts as a minor net source of heat to the water column, providing about 5 MJ m^{-2} of heat over a fortnight. During the winter, however, the sediment bed is a net sink, absorbing about -25 MJ m^{-2} of heat over a fortnight. The relationship between the phasing of the exposure of the flats and the incident shortwave radiation is clearly seen in panels (a) and (b) of Figure 7.

While the net Q_{sw} is slightly positive (from the sediment to the water) during the summer, the fluxes are modulated by the tidal signal: positive during spring tides and negative during neap tides. During spring tides maximum exposure and solar radiation are in phase, while during neap tides minimum exposure and solar radiation are in phase. Each tidal cycle, heat is transferred to or lost from the water at high tide depending on the conditions of the previous low tide. The opposite fortnightly signal is evident during the winter, and the net effect is a loss of heat from the water column to the sediment surface.

The effects of the coincidence of flat exposure and daytime solar radiation are even more apparent at Willapa Bay, as shown in Figure 8. Incident shortwave radiation during March is 70% of the July values, because it is late in the winter, but the seasonal difference is still evident. The net cumulative heat flux during the July fortnight is only about +2 MJ m^{-2}, while net cumulative heat flux during the March fortnight is about -25 MJ m^{-2}.

3.2. Heat fluxes at the leading edge of the flood front

During the summer period at Skagit Bay, observed water column temperatures immediately after inundation are ≈ 5°C warmer than the sediment surface temperatures. Figure 9 shows this phenomena by tidally phase-averaging temperatures, using time after inundation, from 13-18 July at Skagit Bay and 21-28 July at Willapa Bay. These time periods were chosen as they represent the period of maximum exposure at these sites and hence the strongest signals for heating at the leading edge. These leading edge water temperatures exceed the sediment temperatures at both up-flat and down-flat locations, implying that the source of heat cannot be from the sediment. The most likely mechanism is solar heating, which for a thin fluid is a strong function of absorption.

To examine the effects of solar absorption at the leading edge of the flooding front, the thermodynamic model was run for two different light extinction coefficients: $K_d = 1$ m^{-1} and $K_d = 1000$ m^{-1}. Model results are included in Figure 9, in which the high K_d values successfully reproduce the general trend of the data. In particular, high K_d values cause the thin leading edge of flooding water to warm well above the sediment temperatures. In contrast, low K_d values do not reproduce the leading edge temperature.

The effect of solar absorption is most evident in the 20 minutes (≈0.3 hours) after the inundation, when water column temperatures are 4 °C greater during the high K_d runs.

However, the high value of K_d also is important for reproducing the correct sediment temperatures at longer times. This is because any solar radiation not absorbed by the water will go into the sediment. For example, at Skagit Bay, the low K_d values result in a spurious warming of the sediments. This spurious warming creates an accumulating bias in the model results and dramatically increases the RMSE between model and data. The high value of K_d is required to match the data over fortnightly periods, and by extension, to correctly infer seasonal cumulative heat fluxes.

The tidal phasing that creates net heating or cooling also amplifies the effect of solar absorption. During neap tides, the flats are preferentially inundated when the solar radiation is largest, and thus high K_d values notably increase the water temperatures. This is consistent with the observations. For example, at Skagit Bay in the summer, the neap tide water mid-day temperatures are about 25 °C, compared with the spring tide water temperatures at 18 °C (see Figure 3).

At Willapa Bay, the high K_d value is similarly important in matching the observed temperatures at both short and long time scales, however the water temperature does not exceed the sediment temperature during the initial arrival of the flood (see Figure 9). Rather, the water and sediment are in near-equilibrium most of the time. This is likely related to the much higher water content of the muddy sediments at Willapa Bay, compared with the sandy sediments at Skagit Bay. This contrast in composition is consistent with the Willapa tidal flats having properties much closer to that of water *Thomson* [2010].

4. Discussion

4.1. Model sensitivity to λ_s, H_{sw}, and T_{sea}.

The model results indicate that sediment and water column temperatures can be accurately predicted using a sediment-water heat flux coefficient and without the need of sediment temperatures at significant depths. The sensitivity of the results to λ_s, H_{sw}, and T_{sea} was tested by varying these parameters and calculating RMSE for the predicted sediment and water temperatures. Tables 1 and 2 lists the RMSE deviations for these temperatures at Skagit Bay and Willapa bay respectively. RMSE values vary slightly over the observed range of empirically determined (via regression) H_{sw}. As H_{sw} determines the rate at which the sediment and water exchange heat, it is likely that this parameter is most important in determining temperatures immediately after inundation and becomes less important as the water and sediment temperatures equilibrate. There seems to be little significant difference between the choice of H_{sw} at either site.

The importance of the offshore boundary condition is evident by the greatest variability in RMSE under changes of T_{sea}. For the short time periods modeled in this study, constant T_{sea} values were sufficient, but long term measurements would be required to accurately model annual changes or climate senarios.

4.2. K_d and turbidity

High K_d values are necessary to accurately model the post-inundation water and sediment temperatures. The strong absorption of solar radiation is consistent with visual observations (in the field) of extremely high turbidity, especially in the first stage of the flood. Aerial photos from Skagit flats, in particular, have shown a leading edge of turbid water, often repeated by a second line of turbid water. This likely is related to the second peak in water temperature 0.5 hours after inundation at Skagit Bay (see Figure 9). Such heterogeneity is not captured in the model, which uses a constant K_d. It is likely that along flat convergence during the flood tide or the effects of river outflow, processes not included in the model, create a double peak in turbidity that causes enhanced absorption of shortwave radiation. Although these details are not captured, the model does identify the mechanism of solar absorption in water as controlling much of the thermodynamics.

The high K_d value used replicate the enhanced water temperatures of the advancing flood are an order of magnitude above the greatest values (100 m^{-1}) reported for just the infrared portion of the incoming radiation. Most observations of light extinction coefficient occur in water depths O(1-10m) where back-radiation of shortwave energy is less than 1% of the incoming radiation [*Stefan et al.*, 1983]. Considering the extremely shallow, centimeter scale flows that occur at the edge of the flooding front, it is likely that back-radiation and reabsorption of shortwave radiation occurs causing the simple one-directional model of Eq. 12 to under predict the fraction of shortwave radiation absorbed by the water column and hence require larger extinction coefficients.

5. Conclusion

A simple model of cross-shore tidal flat heat transport captures the basic patterns of temperature variations in both the water column and sediment bed for muddy and sandy sites during winter and summer months. Sediment-water heat fluxes are an important component of the heat budget, representing up to 20% of the incoming solar radiation and being larger than latent and sensible heat fluxes. The phasing of tidal flat exposure and daylight is important in controlling the sediment-water heat exchange. During the summer months, net heat flux is from the sediment bed to the water column as the longest periods of exposure occur during the daytime and result in the uptake of heat by the tidal flats. The heat stored in the flats is then released to the water column during inundation. Under winter conditions, the phasing is reversed with maximum flat exposure occurring during the night time, causing a loss of heat to the atmosphere and a net transfer of heat from the water column to the sediment.

The model reproduces temperature observations on tidal, fortnightly, and seasonal time scales. On tidal time scales, a controlling process is the absorption of the shortwave radiation by water. Consistent with observations of high turbidity, the absorption must be near-total for the model to match the temperature observations. The high water temperatures of the initial flooding front create subsequent negative values of Q_{sw} (i.e., heat going from water to sediment). After passage of the initial front, however, sediment-water heat transfer reverses, with the water gaining heat from the sediment bed. Without high extinction coefficients, the shortwave radiation is transmitted through the shallow water column and absorbed by the seabed. This incorrectly heats the sediments instead of the water.

Acknowledgments. Thanks to Chris Chickadel and Alex Horner-Devine for valuable discussions. Thanks to Alex deKlerk and Joe Talbert for help with field data collection. Thanks for AgWeatherNet for meteorological data. This research was supported by the Office of Naval Research.

References

Amos, C. L. (1995), Siliclastic tidal flats, in *Geomorphology and Sedimentology of Estuaries*, edited by G. M. E. Perillo, pp. 273–306, Elsevier, Amsterdam.

Andrews, R. (1965), Modern sediments of Willapa Bay, Washington: A coastal plain estuary., *Tech. rep.*

Boldt, K. V., C. A. Nittrouer, and A. S. Ogston (2013), Seasonal transfer and net accumulation of fine sediment on a muddy tidal flat: Willapa Bay, Washington, *Continental Shelf Research*, doi:10.1016/j.csr.2012.08.012.

Cahill, B., O. Schofield, R. Chant, J. Wilkin, E. Hunter, S. Glenn, and P. Bissett (2008), Dynamics of turbid buoyant plumes and the feedbacks on near-shore biogeochemistry and physics, *Geophys. Res. Lett.*, *35*(10), L10,605, doi:10.1029/2008GL033595.

Cho, Y.-K., M.-O. Kim, and B.-C. Kim (2000), Sea fog around the Korean Peninsula, *Journal of Applied Meteorology*, *39*(12), 2473–2479.

Colijn, F., and V. de Jonge (1984), Primary production of microphytobenthos in the Ems-Dollard Estuary., *Marine Ecology Progress Series*, *14*(2), 185–196.

Friedrichs, C. T. (2012), Tidal flat morphodynamics: A synthesis, *Treatise on Estuarine and Coastal Science*, *3*.

Guarini, J., G. Blanchard, P. Gros, and S. Harrison (1997), Modelling the mud surface temperature on intertidal flats to investigate the spatio-temporal dynamics of the benthic microalgal photosynthetic capacity, *Marine Ecology Progress Series*, *153*, 25–36, doi:10.3354/meps153025.

Harrison, S. (1985), Heat exchanges in muddy intertidal sediments: Chichester harbour, West Sussex, England, *Estuarine, Coastal and Shelf Science*, *20*(4), 477–490, doi:10.1016/0272-7714(85)90090-3.

Incropera, F. P., and D. P. DeWitt (2002), *Introduction to Heat Transfer*, 4th ed., John Wiley & Sons, New York.

Jerlov, N. G. (1976), *Marine Optics*, Elsevier, Amsterdam.

Kim, T.-W., Y.-K. Cho, and E. P. Dever (2007), An evaluation of the thermal properties and albedo of a macrotidal flat, *J. Geophys. Res.*, *112*, doi:10.1029/2006JC004015.

Kim, T.-W., Y.-K. Cho, K.-W. You, and K. T. Jung (2010), Effect of tidal flat on seawater temperature variation in the southwest coast of Korea, *J. Geophys. Res.*, *115*, doi:10.1029/2009JC005593.

Losordo, T. M., and R. H. Piedrahita (1991), Modelling temperature variation and thermal stratification in shallow aquaculture ponds, *Ecological modelling*, *54*(3-4), 189–226, doi:10.1016/0304-3800(91)90076-D.

May, P. W. (1986), A brief explanation of Mediterranean heat and momentum flux calculations, *Tech. Rep. NORDA Code 322*, NSTL Station, Miss.

McBride, A., K. Wolf, and E. Beamer (2006), Skagit Bay nearshore habitat mapping, *Skagit River System Cooperative, LaConner, WA*.

Pavel, V., B. Raubenheimer, and S. Elgar (2012), Processes controlling stratification on the northern Skagit Bay tidal flats, *Continental Shelf Research*, pp. 1–10, doi:10.1016/j.csr.2012.06.012.

Stefan, H. G., J. J. Cardoni, F. R. Schiebe, and C. M. Cooper (1983), Model of light penetration in a turbid lake, *Water Resources Research*, *19*(1), 109–120.

Thomson, J. M. (2010), Observations of thermal diffusivity and a relation to the porosity of tidal flat sediments, *J. Geophys. Res.*, *115*(C5), doi:10.1029/2009JC005968.

Yanagi, T., K. Sugimatsu, and F. FIXME (2005), Effect of tidal flat on the thermal effluent dispersion from a power plant, *J. Geophys. Res.*, *110*(C3), C03,025, doi:10.1029/2004JC002385.

Table 1. RMSE error estimates for the Skagit Bay site. Bold numbers indicate values used for the "best" model runs.

	λ_s (W m^{-1} K^{-1})				H_{sw} (W m^{-2} K^{-1})				$T_{sea}(^{\circ}C)$				
	1	5	8	10	5	10	15	20	6	8	10	12	14
Water July	2.85	2.64	**2.54**	8.04	2.77	2.63	**2.54**	2.48	-	4.06	3.09	6.69	**2.54**
Sediment July	6.06	3.57	**2.72**	2.87	2.73	2.73	**2.72**	2.71	-	1.83	2.06	2.28	**2.72**
Sediment January	5.53	4.21	**3.98**	3.88	4.69	4.37	4.14	**3.98**	5.04	4.68	4.32	**3.98**	-

Table 2. RMSE error estimates for the Willapa Bay site. Bold numbers indicate values used for the "best" model runs.

		λ_s (W m^{-1} K^{-1})				H_{sw} (W m^{-2} K^{-1})				$T_{sea}(^{\circ}C)$					
		1.5	3	5	7	5	10	15	20	4	6	8	10	12.5	15
Water	July	4.49	4.47	4.46	**4.46**	**4.46**	4.41	4.37	4.35	-	-	-	8.05	6.12	**4.46**
	March	2.98	2.93	2.91	**2.90**	**2.90**	2.87	2.84	2.82	3.89	3.01	**2.90**	3.63	-	-
Sediment	July	5.11	4.14	3.73	**3.56**	**3.56**	3.60	3.65	3.71	-	-	-	3.76	3.64	**3.56**
	March	2.38	1.62	1.17	**0.96**	**0.96**	0.93	0.91	0.90	1.21	1.04	**0.96**	0.99	-	-

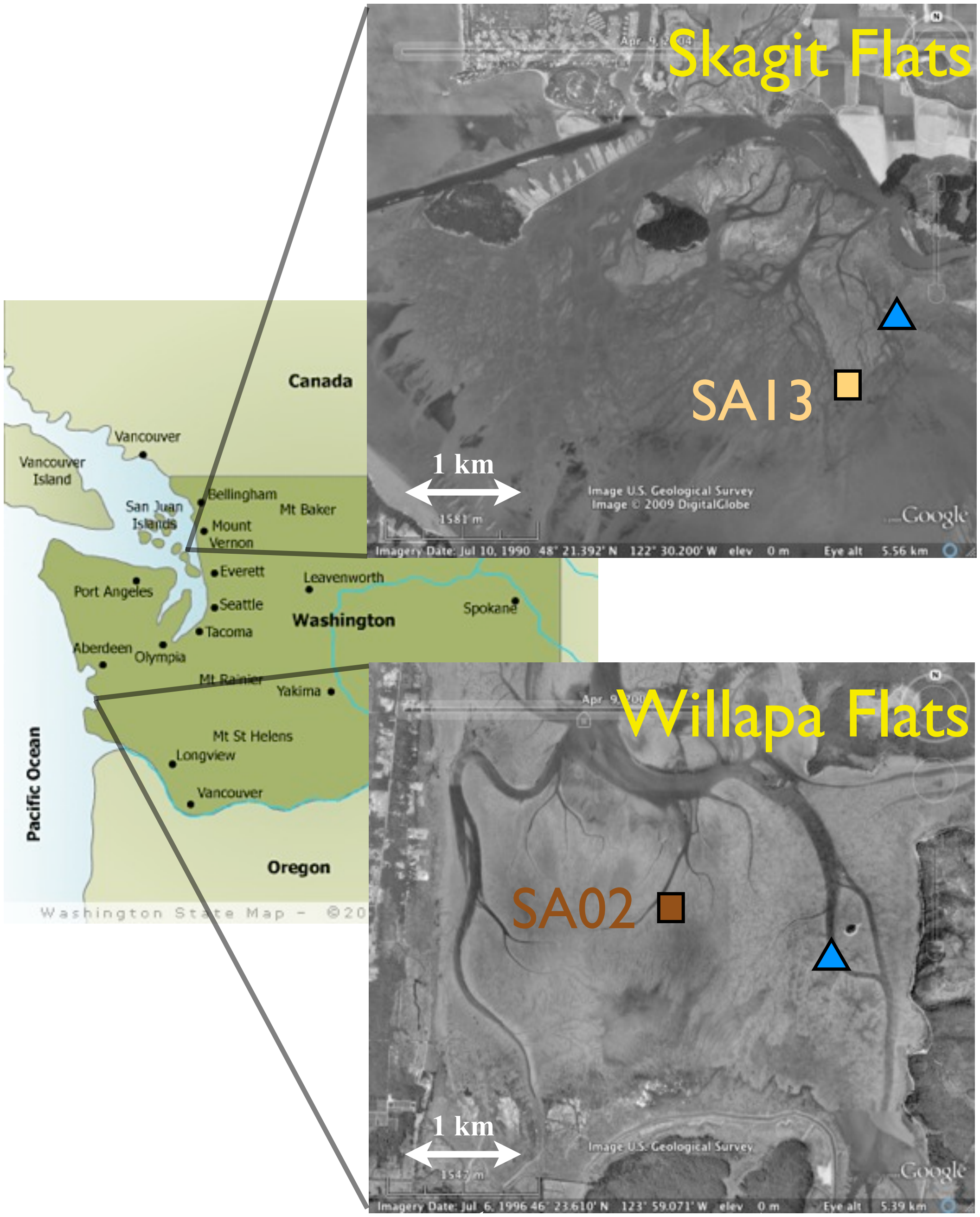

Figure 1. Location of field observations at Skagit Bay and Willapa Bay, WA, USA. Squares indicate the sand anchor locations at each site. Triangles are the locations of the HOBO Met station. Figure modified from *Thomson* [2010]

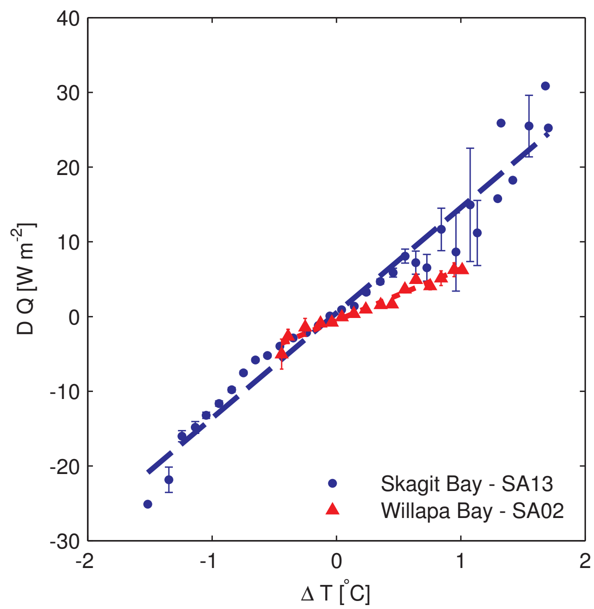

Figure 2. Example fit for h_{sw} for Skagit Bay (S01,S13,S15) and Willapa Bay (W01,W02). dQ is the heat difference as calculated by Eq. 22. Data have been binned into 0.1 °C intervals with the vertical error bars showing the standard error in dQ for each bin.

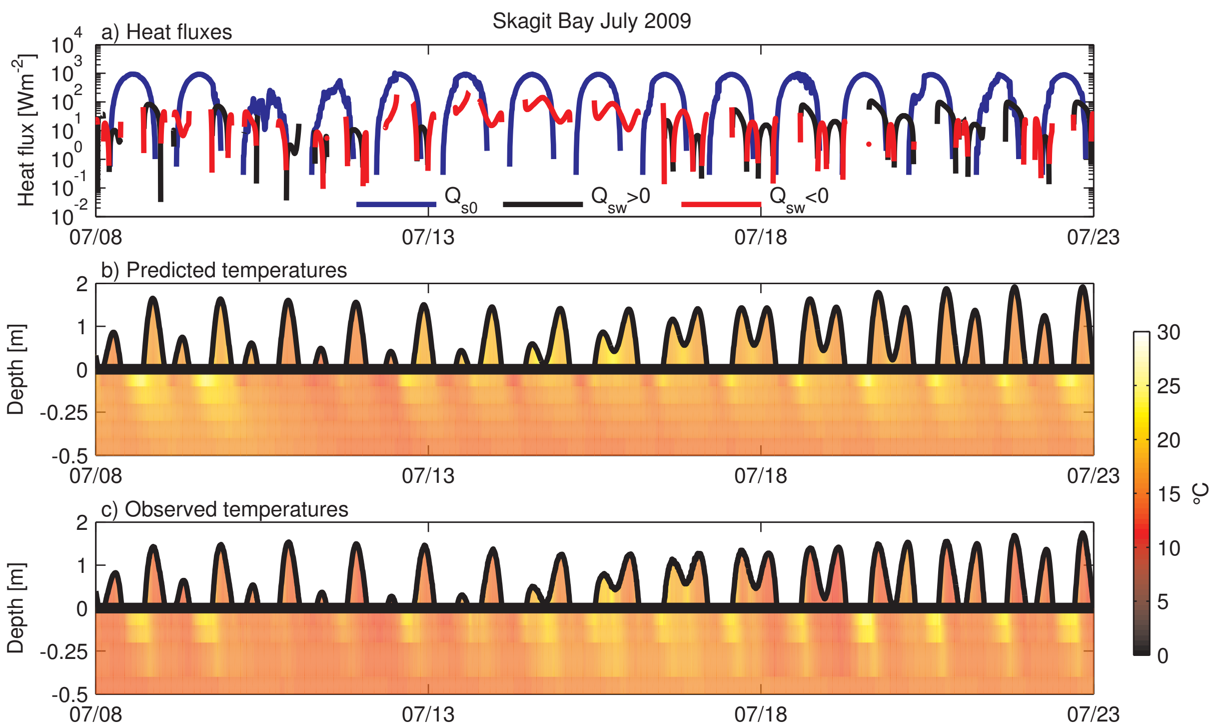

Figure 3. Modeled and observed results for 9-24 July 2009 at Skagit Bay S13. (a) Observed incoming shortwave radiation Q_{s0} (yellow), and modeled sediment-water heat fluxes Q_{sw} (red/black). Black lines indicate positive (into water) fluxes while red lines are negative (into sediment) fluxes. (b) Modeled and (c) observed sediment and water column temperatures. The sediment bed is represented by negative depths and is exaggerated 4x.

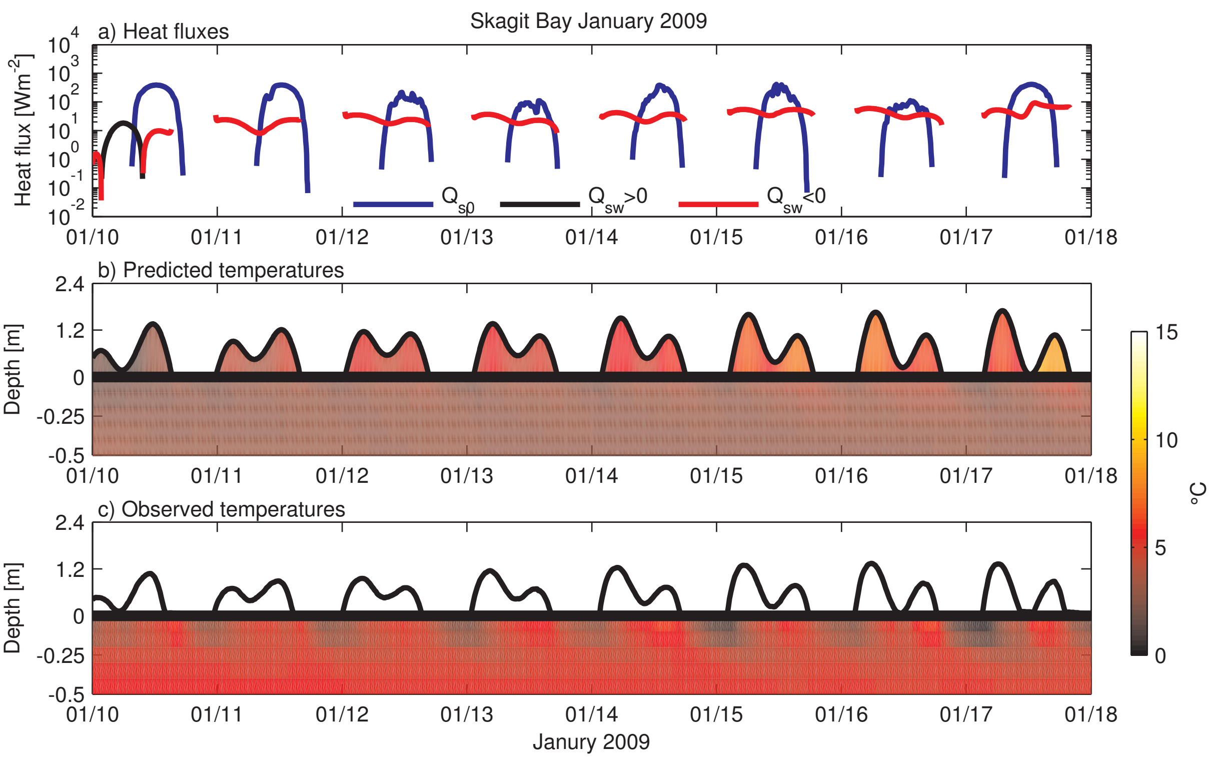

Figure 4. Modeled and observed results for 10-20 January 2009 at Skagit Bay S13. (a) Observed incoming shortwave radiation Q_{s0} (yellow), and modeled sediment-water heat fluxes Q_{sw} (red/black). Black lines indicate positive (into water) fluxes while red lines are negative (into sediment) fluxes. (b) Modeled and (c) observed sediment temperatures. The sediment bed is represented by negative depths and is exaggerated 4x. Water column observations were unavailable for this period.

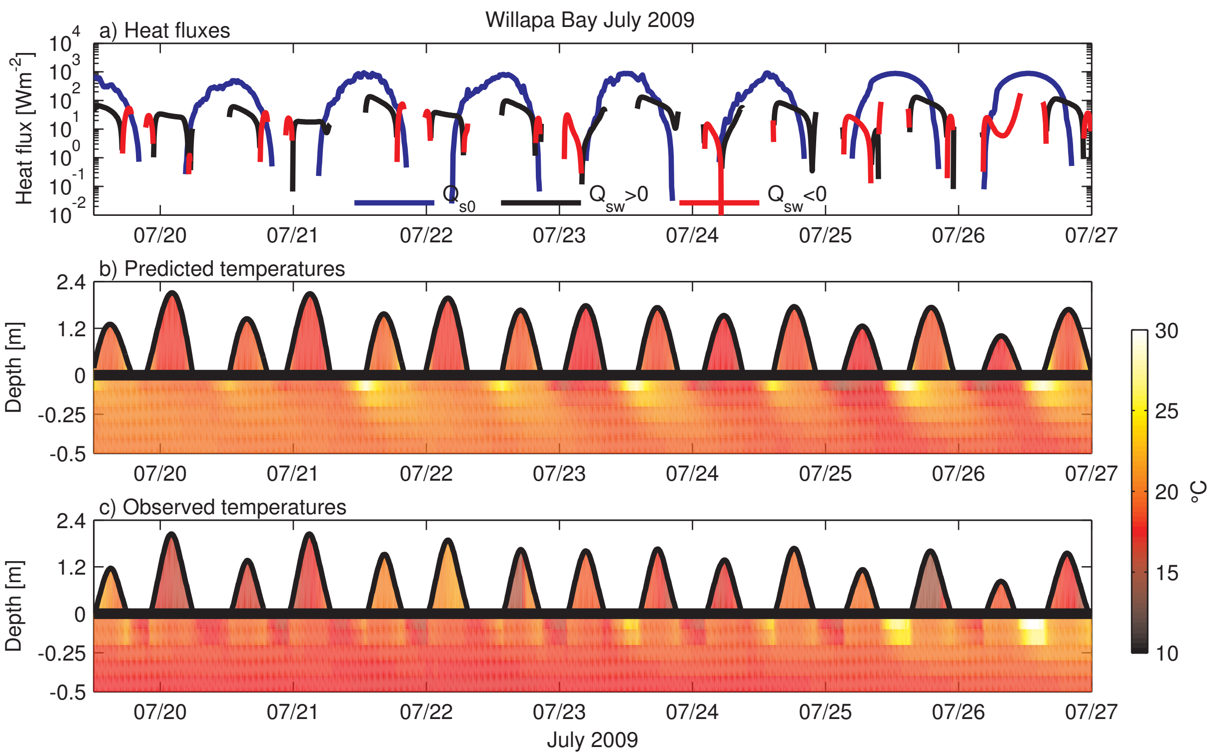

Figure 5. Modeled and observed results for 21-28 July 2009 at Willapa Bay W02. (a) Observed incoming shortwave radiation Q_{s0} (yellow), and modeled sediment-water heat fluxes Q_{sw} (red/black). Black lines indicate positive (into water) fluxes while red lines are negative (into sediment) fluxes. (b) Modeled and (c) observed sediment and water column temperatures. The sediment bed is represented by negative depths and is exaggerated 4x.

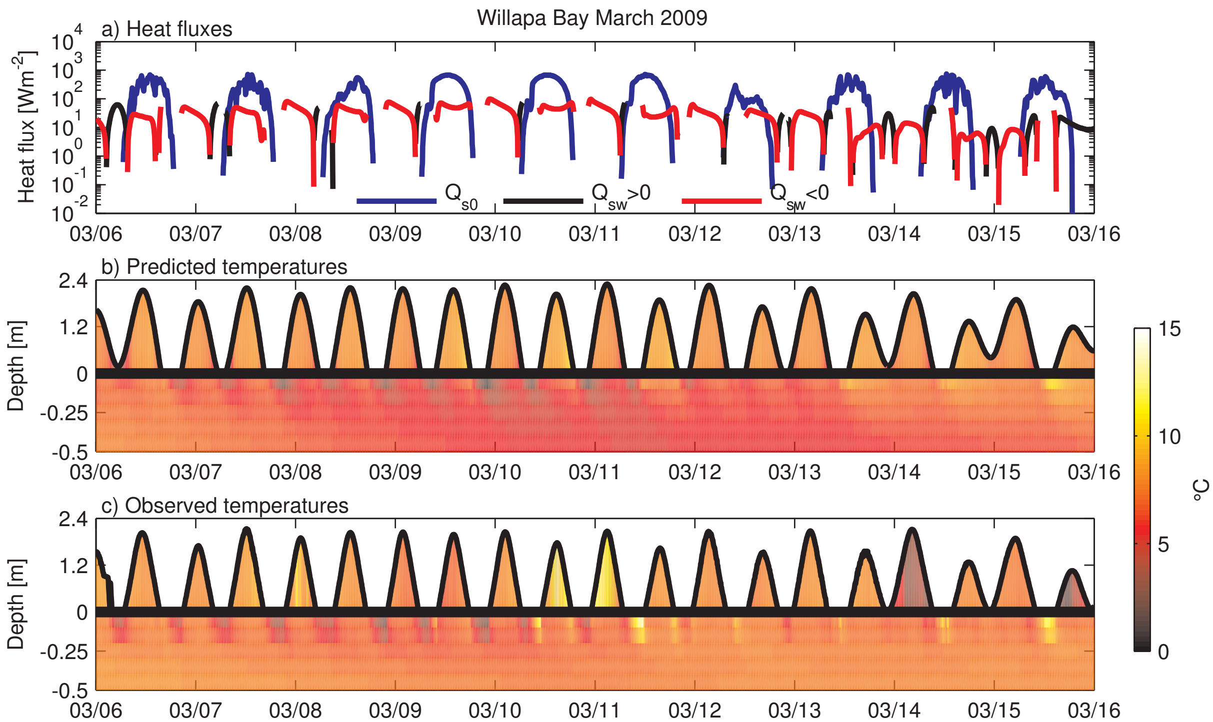

Figure 6. Modeled and observed results for 6-16 March 2009 at Willapa Bay W02. (a) Observed incoming shortwave radiation Q_{s0} (yellow), and modeled sediment-water heat fluxes Q_{sw} (red/black). Black lines indicate positive (into water) fluxes while red lines are negative (into sediment) fluxes. (b) Modeled and (c) observed sediment and water column temperatures. The sediment bed is represented by negative depths and is exaggerated 4x.

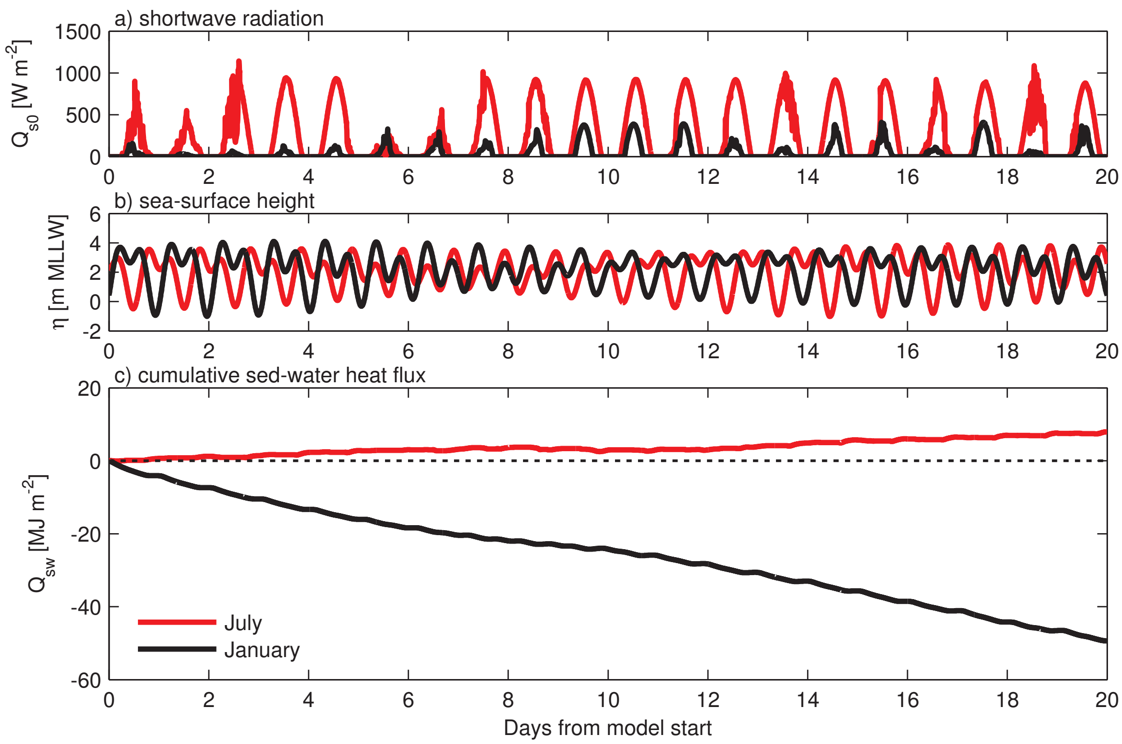

Figure 7. Modeled (a) Solar shortwave radiation, (b) sea-surface height, and (c) cumulative sediment-water heat fluxes for July (red lines) and January (black lines) 2009 at Skagit Bay S13.

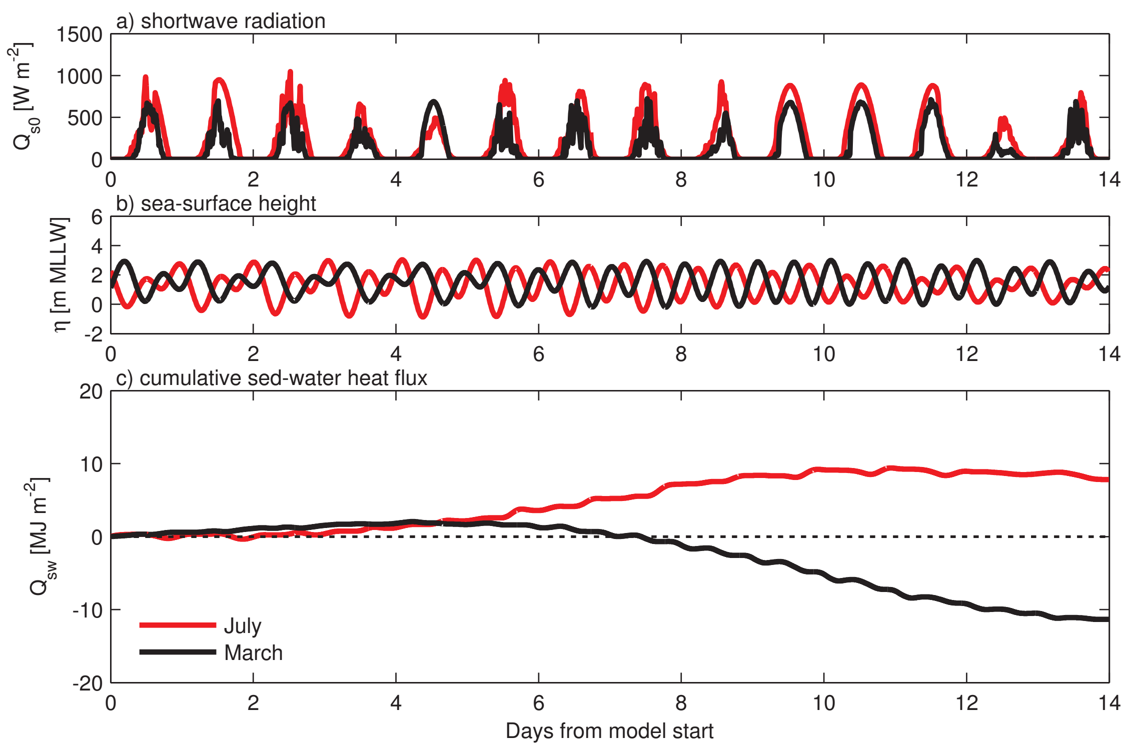

Figure 8. Modeled (a) Solar shortwave radiation, (b) sea-surface height, and (c) cumulative sediment-water heat fluxes for July (red lines) and March (black lines) 2009 at Willapa Bay S02.

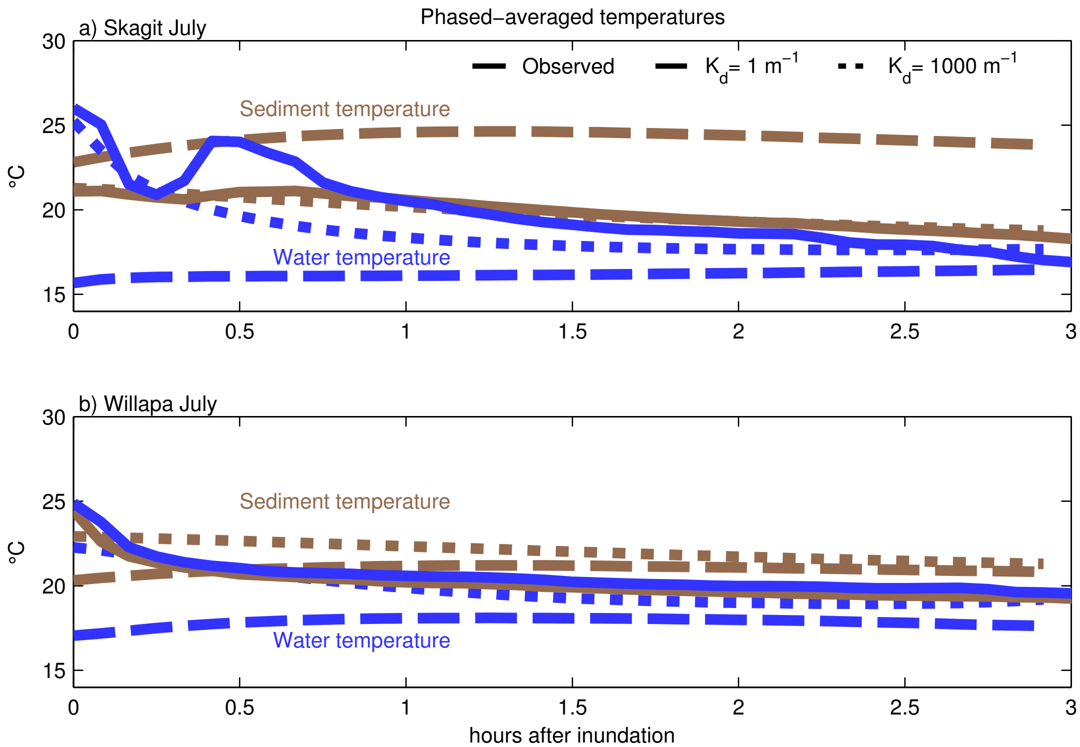

Figure 9. Tidally phase-averaged water (blue) and sediment (brown) surface temperatures for (a) 13-18 July 2009 at Skagit Bay and (b) 21-28 July 2009 at Willapa Bay. The x-axis increases from 0 at the time of inundation to 3 hrs after inundation. Solid lines are the observed temperatures, dashed lines indicate an extinction coefficient of K_d =1000 m^{-1}, and dotted lines K_d = 1000 m^{-1}.